Erosion of the molecular network in the amorphous layers of polyethylene upon high- strain deformation

Zbigniew Bartczak, Magdalena Grala, Emmanuel Richaud, Krystyna Gadzinowska

Erosion of the molecular network in the amorphous layers of polyethylene upon high- strain deformation

Zbigniew Bartczak [a, *], Magdalena Grala [a], Emmanuel Richaud [b], Krystyna Gadzinowska [a]

[a] Centre of Molecular Macromolecular Studies, Polish Academy of Sciences, Sienkiewicza 112, 90-363 Lodz, Poland
[b] Arts et Metiers ParisTech, Laboratoire de Procédés et Ingénierie en Mécanique et Matériaux (PIMM), CNRS, UMR 8006, 151 Boulevard de l'Hopital, 75013 Paris, France

Keywords:
Semicrystalline polymer
Polyethylene
Plastic deformation
Molecular network
Entanglements

A B S T R A C T

Samples of linear polyethylene, neat and crosslinked by irradiation with electron beam, were subjected to heavy plastic deformation by plane-strain compression up to the true strain exceeding 2 (deformation ratio $\lambda > 8$) at room temperature. Structural studies of deformed samples and investigation of long-term strain recovery demonstrated that the deformation of the neat, non-crosslinked HDPE is completely reversible above the melting point of the crystalline phase, provided that the applied true strain does not exceed $e = 1.0$ ($\lambda = 2.7$). At higher applied strains, $e > 1$, an irreversible deformation component emerged gradually, and at $e = 2.1$ ($\lambda = 8.2$), the permanent, truly irreversible, residual strain was approx. $e_{res} = 0.36$ ($\lambda = 1.4$). In contrast, samples of crosslinked HDPE above T_m exhibited complete reversibility of deformation, irrespectively of an applied strain, and $e_{res} \approx 0$. The source of permanent irreversible strain component in neat HDPE is a deformation-induced partial destruction of the molecular network of entangled chains within amorphous interlamellar layers. The principal mechanism found was chain disentanglement, which was supplemented by a very limited chain scission. In the case of crosslinked materials, the dense and relatively homogeneous molecular network appeared robust enough to avoid any damage. Consequently, the strain appeared here fully reversible upon melting of crystalline phase.

1. Introduction

Semicrystalline polymers can deform to very high strains. Their deformation is a complex and multi-level process due to complicated hierarchical structure. A variety of mechanisms operate at different levels of the structure and the process of deformation is strongly dependent on the underlying microstructure of the material. Any macroscopically homogenous deformation is accommodated by cooperative action of these mechanisms in the heterogeneous multi-level structure.

The microstructure of semicrystalline polymer is commonly described by a two-phase model consisting of randomly oriented crystalline lamellae stacks intercalated with amorphous layers. At this level, the basic micromechanisms of deformation of crystals and amorphous phase are considered. It has been well established that the principal mechanisms involved in the plastic deformation of polymer crystals are crystallographic in nature, primarily crystallographic slip that appears active at all strain levels [1,2]. For the amorphous phase, it was found that the shear of amorphous interlamellar layers was the principal deformation mechanism. It plays a very important role in the deformation sequence, not only allowing for a high orientation of amorphous component, but also influencing deeply the deformation of crystalline phase, since both phases are intimately connected through many chains crossing the crystalline/amorphous interface, therefore both components can deform only simultaneously and consistently [2]. This implies that amorphous phase, in spite of compliance much higher than crystals (at $T > T_g$), can deform independently only in a very limited extent. Consequently, at the initial and moderate stages, deformation of amorphous layers merely follows deformation of adjacent crystalline lamellae [3–6]. Situation changes at high strains, when increasing rubber-elastic stresses generated upon advanced shear deformation of amorphous layers become higher than stresses accompanying deformation of crystalline phase, much less dependent on strain [7]. From this point on, the interlamellar shear of amorphous component takes control over the process of further deformation, and deformation of crystals now only accommodates to strain increment of the amorphous phase. During the early and

* Corresponding author.
E-mail address: bartczak@cbmm.lodz.pl (Z. Bartczak).

moderate stages of deformation, crystals become distorted but the crystalline lamellae remain undestroyed, whereas at larger strains, the original crystalline microstructure frequently breaks down due to advanced slip and a high stress generated in adjacent amorphous layers and transmitted to crystals. Consequently, a new fibrillar structure is formed [8,9].

The mechanical response of an amorphous phase is determined by its topological structure, including chains crossing interfaces with neighboring lamellae (as e.g. tie-molecules, loose loops or cilia) and a molecular network of entangled chains [10]. In this molecular network, chain segments immobilized at interfaces constitute *quasi*-solid crosslinks, while entanglements represent crosslinks of a certain mobility, which ultimately, at some conditions, can be even resolved (chains disentangled). It is already well understood that strain hardening in amorphous polymers originates from the network structure [11–13]. The same is actually true for semicrystalline polymers, since their deformation can be considered as a simultaneous deformation of two co-continuous interlaced network-like structures: a skeleton made up of crystallites interconnected with the interlamellar layers of entangled amorphous phase [4], deformation of which is supposed to proceed in a similar fashion as deformation of an amorphous polymer, including the rubber-like behavior above the glass transition temperature. Deformation of molecular network within amorphous layers is finite, limited by the length of segments between crosslinks, primarily entanglements. Deformation of amorphous layers should manifest then in a very high stress response to large strain [7], especially when approaching the network extensibility limit, and high reversibility of deformation, which in fact is frequently observed experimentally [10,14,15].

Strobl et al. [4–6,16,17] demonstrated that the properties of the molecular network influence deeply the deformation behavior of semicrystalline polymers. They proposed a strain-controlled deformation scheme of semicrystalline polymers, in which two of the critical strains, controlling the deformation sequence (points C and D at the true strain around $e = 0.6$ and $e = 1$, respectively [4]), are related to the response of the molecular network. According to this scheme, stretching of the sample leads to a gradual orientation of the amorphous chains along the drawing direction that obviously decreases the entropy of the amorphous phase. A retracting force is generated since the system tends to recover an isotropic state of optimized entropy [18]. This force generated in the deformed network of entangled chains within interlamellar layers is transferred to neighboring crystallites by macromolecular chains linking both phases. At the point C, at true strain of approx. 0.6, the stress acting on crystalline lamellae reaches a critical value above which they are no longer stable and undergo fragmentation, which eventually leads to partial destruction of the initial morphology and replacing it by the fibrillar structure. Finally, with a further progress of deformation, the entangled network of amorphous phase approaches its extensibility limit, which results in a strong rise of the stress. That leads to another transition, manifesting in a decreasing amount of strain recovered upon sample unloading, found above the true strain of 1–1.2 (λ~3; point D of the Strobl's scheme). This transition was postulated to be a result of intensified crystal fragmentation and presumably chain disentanglement beginning in amorphous phase that should lead to a partial disintegration of the molecular network [4]. Our previous studies supported the Strobl's view on the deformation sequence and confirmed a direct correlation between concentration of entanglements and the deformation behavior, especially at high strains, in the strain hardening range, [3,10,15,19,20]. Model calculations [7] as well as experimental studies of the post-deformation relaxation behavior of compressed polyethylene [10] indicated that the rubber-like network stress, a sub-component of the observed elastic part of the stress, increases substantially at high strains, above the true strain of $e = 1.0$, and is evidently the main source of the strong strain hardening of the sample. Moreover, the contributions of rubber-like recoverable deformation and permanent plastic flow depend directly on the actual network density, which is possibly reduced at high strain due to resolving of entanglements [19]. Investigation of a broad range of samples of polyethylene homo- and copolymers [10,15] demonstrated that the response of the molecular network of entangled chains in amorphous layers change significantly above of $e = 1$ for all materials studied. In samples deformed below this strain, a significant part of the applied strain appeared recoverable, especially upon heating close to the melting point (even a nearly complete recovery was observed in an ethylene copolymer of very low crystallinity). Above $e = 1$, the contribution of the permanent (unrecoverable) strain component was observed to increase gradually with an advance of applied strain. Such behavior could suggest a strain-induced progressive destruction (erosion) of the molecular network, beginning at $e = 1$. The postulated mechanism of network erosion was either (i) disentanglement or (ii) scission of highly stretched chains, both leading to some reduction of the network density and hence a partial relaxation of the network. That relaxation allows further deformation of the amorphous phase, already deformed nearly to its extensibility limit. Even if the mechanism (i) involving disentanglement sounds attractive, it may not be a principal mechanism because large translations of chains is required to resolve completely an entanglement knot, especially when located in the mid-length of the chain and the molecular weight is high. The flow produced by interlamellar shear can appear then sufficient only for resolving entanglements of relatively short chains or those entanglements that are located close to the chain ends in long chains. On the other hand, it seems that the complete resolution of numerous entanglements is not required to change the network properties, and much more probable translations of mobile entanglements along the chain can be sufficient to increase distances between crosslinks and modify response of the network. The second postulated mechanism – the scission of primary bonds in the main chain needs a high local stress along the chain in order to break the very strong C–C bonds in the chain backbone. This implies a very high stress in the sample, which is possible only in the final deformation stages of the most intense strain hardening and fracture. Chain scission was detected experimentally in several semicrystalline polymers to occur mainly on fracture. Both direct (ESR detecting directly the free radicals, see e.g. Refs. [21,22]) and indirect methods (as reduction in average molar mass [23–25] or increase of concentration of end-groups determined with IR spectroscopy [23,26–28]) were used. For plastic deformation prior to fracturing, the chain scission mechanism was excluded as a major contributor to the plastic deformation [29–31], although some reports indicated its occurrence upon a very heavy deformation [32].

A large number of material models were developed to predict the mechanical response of amorphous polymers (see e.g. Ref. [33] for the review). More recently, the mechanical behavior of semicrystalline polymers has been also extensively modeled (see e.g. Ref. [34] for references). Many efforts have been carried out to describe their complex mechanical behavior at large strains, considering also a possible contribution of chain disentanglements. For example, the model developed recently by Billon predicts that entanglements initially are not mechanically active and act as crosslinks at low stress/strain, then with increasing strain energy they gain a certain level of mobility that induces visco-elasticity and from a certain limit of energy they gain in mobility, which corresponds to disentanglement and visco-plasticity at high strain [34,35].

The aim of the present study was to investigate the deformation and post-deformation recovery behavior of linear polyethylene, taken as a representative semicrystalline polymer, particularly in relation to the properties of the molecular network within amorphous phase. The most important question was how much that network is altered by a severe deformation and what are the underlying mechanisms. Similarly to our previous studies [3,15,19], the plane-strain compression was chosen as a deformation mode due to its advantages over other deformation modes [3], primarily its stability and inhibition of any unwanted side-effects as e.g. cavitation, commonly occurring on tension. Cavitation can be considered as a local fracturing event, thus it must be avoided in studies of plastic deformation. The studies of the deformation performed in this work were focused on the rubbery-elastic response of the amorphous component, possibly influenced by a changing network structure.

2. Experimental

2.1. Materials and sample preparation

The material used in this study was linear high-density polyethylene (HDPE), provided by Basell, with the density of 0.962 g/cm^3, melt flow rate MFR (2.16 kg, 190 °C) = 0.2 g/10min, molecular weight of M_w = 169 300 g/mol, and polydispersity M_w/M_n = 5.9. It was checked by measurements of oxidation induction time (OIT>30min.) that HDPE contains stabilizers, which prevent the generation of chain scissions and unstable oxidation species during polymer processing. Therefore, no additional stabilizers were added.

Samples in the form of 50 × 50 mm plates, 4.5 mm thick, were prepared by compression molding at T = 190 °C and p = 50 bar. The molded plates were solidified by fast cooling in an iced water. All samples were prepared according to the same protocol to obtain similar supermolecular structure.

A part of prepared plates was crosslinked by irradiation with an electron beam of 6 MeV energy. Samples of various crosslink density were obtained by irradiation with different doses: 50, 100 and 200 kGy. Details of the procedure are given in Reference [10].

Specimens of the size desired for deformation experiments were machined out from virgin and irradiated plates. During machining, the skin layers, at least 0.25 mm thick, were removed from both sides of the plates. The specimens cut from the core parts of the plates, used in all experiments, demonstrated quite uniform structure as compared to removed skin layers in which a structure gradient due to fast cooling conditions was observed.

2.2. Deformation and recovery

Plane-strain compression tests were performed using a loading frame of a universal tensile testing machine (Instron, Model 5582, controlled by the Bluehill II software) and a compression fixture of the type of deep channel-die (channel depth of 60 mm), equipped with a LVDT transducer, mounted close to the specimen for precise strain determination. The channel-die tool is shown schematically in Fig. 1. The size of the specimens used were 20 × 50 × 3.85 mm (along the loading direction, LD, the flow direction, FD, and the constrain direction, CD, respectively). The surfaces contacting with the die and the plunger were lubricated to reduce friction during compression. Other details are given in Reference [3]. All deformation experiments were performed at room temperature with the constant true strain rate of $e' = 0.001\ s^{-1}$. The applied strain was determined as the true strain calculated from the reduction of the specimen dimension along the loading direction (specimen height) using the following equation (Hencky measure of strain):

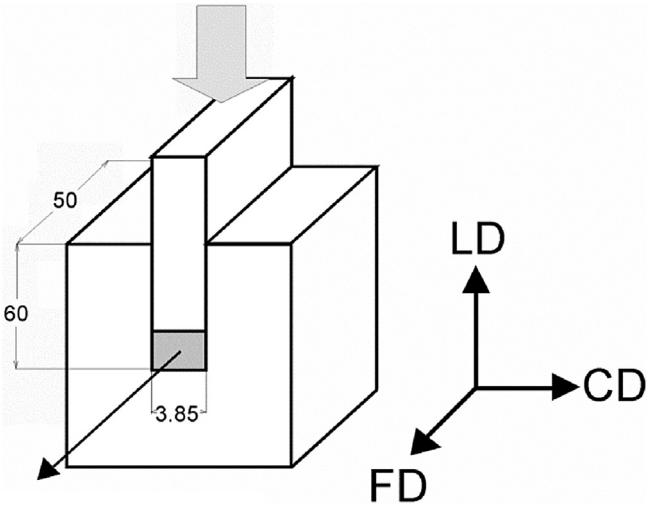

Fig. 1. The deep channel-die used for plane-strain compression. The compressed sample is marked gray. Dimensions are given in mm. The reference directions are the loading direction (LD), flow direction (FD) and the constrained direction (CD).

$$e = \int_{h_1=h_o}^{h_1=h} \frac{dh_1}{h_1} = \ln\left(\frac{h_o}{h}\right) = \ln\left(\frac{h_o}{h_o - \Delta h}\right) = \ln(CR) = \ln \lambda \qquad (1)$$

where h_o denotes the initial and actual specimen height, $h = h_o - \Delta h$ represents its actual height, Δh is the measured displacement of the plunger and $\lambda = CR = h_o/h$ is the compression ratio.

The advantage of a deep channel-die is that the samples produced by compression in such a die are relatively large, so that the structure and orientation produced by plastic deformation as well as the macroscopic recovery behavior could be studied easily.

The post-deformation behavior was monitored over a period of time after compression and unloading. For this purpose, the specimens deformed to the desired true strain were immediately unloaded and taken out of a channel-die to allow their unconstrained recovery. Specimen dimensions along FD, CD and LD were measured repeatedly with a digital micrometer over a period up to 6 months after unloading. The recovered and residual true strain components were calculated from the measured changes of specimen dimensions using Eq. (1). In a separate experiment samples already recovered at room temperature were heated up to the temperature of 110 °C, 123 °C (i.e. just below the onset of melting) or 145 °C (above melting of crystals) and annealed for 30 min. Next, the samples were cooled down, their dimensions were measured and the residual and recovered strain components determined (due to crosslinking samples maintained their shape even after melting of crystals, which allowed determination of the residual strain).

2.3. Characterization

2.3.1. DSC

Thermal analysis was conducted using a TA 2920 DSC apparatus (Thermal Analysis). The melting thermograms were recorded at the heating rate of 10°/min, under nitrogen flow. The crystallinity was estimated on the basis of heat of melting of the sample, assuming the heat of melting of 100% crystalline PE of Δh_f = 293 J/g, [36].

2.3.2. SAXS

The lamellar structure of samples was probed with 2-dimensional small angle X-ray scattering (2-D SAXS). The Kiessig-

type camera with sample detector distance of 1.2 m was coupled to an X-ray CuK$_\alpha$ low divergence microsource, operating at 50 kV and 1 mA (sealed-tube micro-source integrated with multilayer collimation optics, producing a highly collimated beam with a divergence of 0.8 × 0.8 mrad^2; GeniX Cu-LD by Xenocs, France). The collimation optics was combined with 2 additional hybrid scatterless slits systems (Xenocs) placed between the multilayer optics and the sample stage, forming the beam of square cross-section. The two slit assemblies were separated by 1200 mm. The scattering produced by the sample was recorded with the Pilatus 100 K solid-state area detector of the resolution of 172 × 172 μm^2 (Dectris, Switzerland). The long period (LP) of unoriented samples was determined from one-dimensional sections (background and Lorentz corrected) of 2-D patterns using the Bragg's law.

2.3.3. Gel content and swelling

The gel content in irradiated samples was determined by solvent extraction in boiling *p*-xylene (T = 138 °C). The specimen approx. 0.3 g enclosed in the pre-weighted pouch made of 100 mesh stainless steel grid was extracted in 1 dm^3 of boiling p-xylene for the total time of 16 h. To inhibit further crosslinking of the specimen or its degradation 1 wt.% of an antioxidant (Irganox 1010, Ciba-Geigy) was added to xylene. The gel left after extraction was dried in vacuum for 5 h at 80 °C and then weighted. The gel content was calculated using the following equation:

$$g = \frac{W_d}{W_o} \cdot 100\% \tag{2}$$

where W_o is initial weight of the sample and W_d is the weight of an insoluble fraction, left after extraction and drying.

The dried gel, still in the stainless steel pouch used for the gel content determination, was allowed to swell again in boiling p-xylene (T = 138 °C) for a minimum of 4 h. At this point, an equilibrium swelling was presumably achieved. The pouch with swollen sample inside was taken out from the solvent and placed in a pre-weighed weighing bottle with a tight cover. The weighing bottle including cover, steel pouch and the swollen gel was weighed and the mass of the solvent taken up by the gel was calculated. The solvent taken up by the stainless steel basket itself was subtracted from the total amount of solvent taken up. Next, the gel was dried under vacuum at 80 °C for 5 h in order to determine the weight of the dry gel after swelling.

For the calculation of average mass between crosslinks, M_c, from equilibrium swelling measurements the Flory–Rehner equation was used [37],:

$$-\ln(1 - V_r) - V_r - \chi V_r^2 = \frac{\rho_p V_o}{M_c^*}\left(V_r^{1/3} - \frac{V_r}{2}\right) \tag{3}$$

where M_c^* is molar mass between crosslinks (not corrected for loose chain ends), $\chi = 0.31$ is the polymer-solvent interaction parameter for polyethylene and *p*-xylene [38], $V_o = 139.3$ cm^3 is the molar volume for p-xylene [38], and V_r is volume fraction of polymer in the swollen gel calculated from the equation:

$$V_r = \frac{1}{\left(\frac{M_s \rho_p}{M_p \rho_s} + 1\right)} \tag{4}$$

where M_p is the weight of the dry gel, M_s is the weight of the solvent absorbed by gel, $\rho_p = 0.806$ g/cm^3 is density of the polymer [38], and $\rho_s = 0.761$ g/cm^3 is density of the solvent, [38]. Both densities refer to T = 138 °C.

To correct for loose chain ends present in the material, $1/M_c^*$ in Eq. (2) is replaced with the following [37]:

$$\frac{1}{M_c^*} = \frac{1}{M_c}\left(1 - \frac{2M_c}{M_n}\right) \tag{5}$$

where M_c is the molar mass between crosslinks, corrected for loose chain ends and M_n is the number average molecular weight of the polymer prior to crosslinking. The network density, N_x, expressed by the number of elastically active chains between crosslink junctions per unit volume, was calculated from M_c using the equation:

$$N_x = \frac{\rho_p N_A}{M_c} \tag{6}$$

where N_A is the Avogadro's number. For normal crosslinking, in which four chains meet at ach junction point, the number of crosslink junctions is $x = N_x/2$ [18].

The values used for ρ_p, ρ_s, χ and V_o were taken from Ref. [38]. A constant value of the solvent interaction parameter χ was used despite several authors claim that the solvent interaction parameter can depend on the crosslink density [39].

2.3.4. FTiR spectroscopy

The Jasco 6200 FTiR spectrometer (Jasco) was used for measurements. All spectra were recorded in the transmission mode in the range of 400–4000 cm^{-1} at a resolution of 4 cm^{-1} and 256 scans averaged per spectrum. Sections about 0.1 mm thickness cut from internal part of bulk samples and then recrystallized were used for measurements. The peak at 2020 cm^{-1}, a combination amorphous-crystalline band associated with twisting of CH_2 was selected as an internal reference, since it can be regarded as unaffected by minor changes in the polymer structure [40,41]. At the peak at 2020 cm^{-1}, all the spectra were normalized at the absorption of 0.05, correlating to a film thickness of ca. 100 μm. The concentrations of carbonyl and vinyl compounds were calculated from their integral absorbance and respective integral molar extinction coefficients ε (l mol^{-1} cm^{-2}) using the Lambert's law. To perform these calculations, the following extinction coefficients were used: esters (1740-50 cm^{-1}) ε = 10,990, aldehydes (1730-35 cm^{-1}) ε = 5890, acids (1712-15 cm^{-1}) ε = 17,170, unsaturated ketones/esters (1690-1700 cm^{-1}) ε = 4625 [42].

2.3.5. GPC

The molecular weights and molecular weight distribution of the neat and deformed HDPE were determined by high-temperature gel permeation chromatography (GPC; Agilent 220 HT with RI detection) at 135 °C using 1,2,4-trichlorobenzene (CHROMASOLV®, ≥99% grade from Sigma Aldrich stabilized with 0.0125% BHT) as solvent and 1 ml min^{-1} flow rate. Samples were dissolved in TCB at 150 °C during 10 min prior to measurement.

3. Results and discussion

3.1. Structure and morphology of irradiation cross-linked samples

Microscopic observations revealed the same uniform spherulitic morphology in neat and cross-linked samples. Table 1 lists the properties of the crystalline phase, derived from DSC and SAXS data, as well as the gel content in crosslinked samples of HDPE (sample code H-n, where n denotes the absorbed dose), the chemical crosslink network density and an average molecular mass between crosslinks in these samples, estimated from extraction and swelling data of the same material, as well as the effective network density (including solid crosslinks and entanglements) estimated from mechanical data and reported in Ref. [10].

Table 1
Characteristic of samples studied.

Sample (dose)	DSC melting temperature, T_m (°C)	Crystallinity, X_c, [a] (wt.%)	Long period, LP, [b] (nm)	Gel content, [c] (%)	Average molecular mass between chemical crosslinks, M_c, [c] (g/mole)	Chemical crosslink network density, $N_x \times 10^{-26}$, [c] (m^{-3})	Effective network density in solid sample, $N_{eff} \times 10^{-26}$, [d] (m^{-3})
H-0 (0 kGy)	134.1	71.5	24.4	0	–	–	3.7
H-50 (50 kGy)	134.4	70.7	24.5	59	5940	0.82	4.6
H-100 (100 kGy)	134.6	71.3	24.3	69	3790	1.28	5.2
H-200 (200 kGy)	134.1	69.2	24.3	77	1840	2.63	5.7

[a] Determined from the DSC melting peak, $\Delta H_f = 293$ J/g taken for calculations.
[b] LP determined with Bragg's law from 1-D sections of 2-D SAXS patterns.
[c] Taken from Ref. [10], estimations based on swelling data.
[d] Taken from Ref. [10], estimations based on fitting the stress-strain data.

Radiation induced crosslinks are preferentially generated in amorphous phase while a dense and ordered crystalline phase remains practically free of chemical crosslinks. Data presented in Table 1 confirm that view, revealing the melting temperature of PE crystals and the long period both practically independent on irradiation. This implies that also the thickness of crystals does not change after irradiation. Concurrently, only a slight decrease of crystallinity with an increasing irradiation dose can be observed, which indicates that perhaps a very small fraction of crystals was destroyed by radiation treatment. This verifies stability of PE crystals with respect to the applied irradiation dose.

Data presented in Table 1 show also the characteristics of the network. It can be seen that both the insoluble gel content and the network density increase with increasing irradiation dose. The estimated crosslink network density values, N_x are consistent with previously published data [43] and demonstrate a linear dependence on the irradiation dose. Back-extrapolation to the null-dose (virgin sample) gives the value of N_x close to 0. This estimation based on measurements of swelling of the gel samples in p-xylene at T = 138 °C. At such conditions, all entanglements, except of those entrapped between chemical crosslink junctions produced by irradiation, were resolved and disappeared. The extrapolated value of N_x close to zero for the dose = 0 suggests that apparently no entanglements had been trapped permanently between chemical crosslink junctions in the studied HDPE sample of moderate molecular weight. The expected overall density of the network in an irradiated molten sample is roughly $N \approx N_x + N_e$, where N_x is the density of chemical crosslinks, and $N_e \approx 4 * 10^{26}$ m^{-3} [44] is the density of entanglements. In a solid sample however, the amorphous phase can demonstrate a network denser than estimated above since all chemical crosslinks have been created in amorphous part and a significant fraction of entanglements pre-existing in the molten sample was rejected out of growing crystallites and concentrated in the amorphous layers rather than being resolved by crystallization. Therefore, the network density N estimated above ($4–6.6 * 10^{26}$ m^{-3}) can be considered as a lower-bound for amorphous phase in a solid crosslinked HDPE [10]. An upper-bound may be estimated higher, even up to 3 times (i.e. $1.2–2.1 * 10^{27}$ m^{-3}), under a severe assumption that crystallization does not resolve any entanglement, but instead all of them have been concentrated in amorphous layers constituting about 1/3 of the sample volume, together with all chemical crosslinks. In the previous work [10], we estimated the effective network density (both chemical crosslinks and entanglements) by fitting equation of a model amorphous phase to the experimental residual stress vs. strain data. The results of these estimations are presented in the last column of Table 1. The effective network densities appeared only slightly higher than lower-bound estimates discussed above. This implies that a considerable fraction of entanglements pre-existing in the melt prior to crystallization had been resolved during crystallization rather than being swept by growing crystals into amorphous phase, probably owing to a moderate molecular mass of polyethylene studied.

3.2. Stress-strain behavior

The samples of the neat and irradiated HDPE were subjected to plane-strain compression at room temperature and constant true strain rate of e' = 0.001 s^{-1}. Compression was carried out up to either the fracture of the specimen or approaching the load limit of the loading frame (10 kN), whichever happened earlier. From the measured load-displacement data, the true stress-true strain curves were determined. For plane-strain compression in a channel-die, true stress is simply equal to the nominal stress, while true strain can be calculated with Eq. (1). Fig. 2 shows representative true stress-true strain curves.

All obtained curves have the same shape, typically observed in plane-strain compression of a semicrystalline polymers. Moreover, the curve of virgin PE agrees quite well with the true stress-true strain curves obtained in tensile deformation mode for polyethylene of similar molecular characteristics [4,45]. The significant difference between tensile and compression curves can be, however, observed in the strain hardening stage: the samples tested in tension did not show such a strong strain hardening as observed in the plane-strain compression. Besides, they used to fracture in tension at lower strains than in compression. Such a difference in

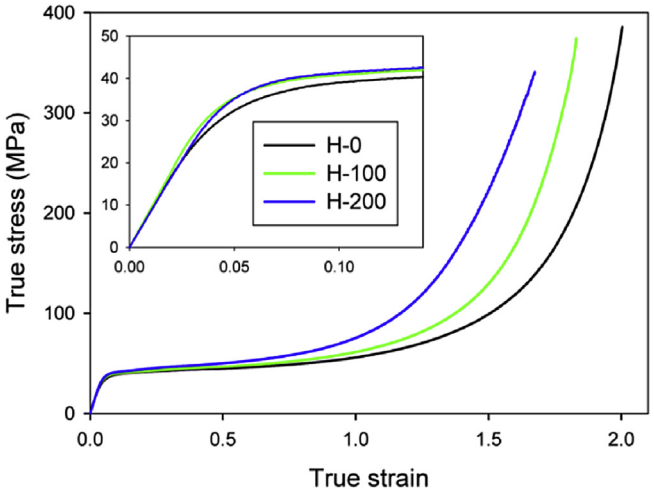

Fig. 2. The true stress-true strain curves of the samples of HDPE irradiated with electron beam of various dose. All samples were deformed at room temperature and with the constant true strain rate of de/dt = 0.001 s^{-1}. Inset shows an initial portion of the same curves.

strain hardening behavior in tension and compression is a result of the less intense fragmentation of lamellae in compression than in tension [46,47], in which the entire lamellar structure is quickly destroyed and replaced by micro-fibrils. Simultaneously, micro-cavitation, while severe in tension, is completely suppressed in plane-strain compression due to external constraints imposed by the die, resulting in a significant compressive stress component. Consequently, the already highly strained lamellar crystals as well as highly extended amorphous material within interlamellar layers are much more constrained than in tension and the sample responds to compression with higher stress than to extension at the same strain. Due to the inhibition of cavitation, the compressed, still continuous material can deform to higher strains than in the tensile mode in which numerous cavities act as flaws leading to an earlier fracture.

The neat and irradiated HDPE samples exhibit similar elastic modulus and yield stress, which reflects their crystalline structure that was practically unchanged by irradiation, since both modulus and yield stress are controlled by the amount and properties of crystalline phase [3,48–51]. On the other hand, one can observe a substantial variation of strain hardening behavior and the ultimate strain with changing irradiation dose – strain hardening sets in earlier and the stress reaches very high ultimate values, above 400 MPa, at considerably lower strain in samples of higher irradiation dose, i.e. exactly as expected for samples of increasing network density [3].

Deformation of the crystalline phase proceeded similarly in all samples, irrespective of crosslinking degree, with the same crystallographic mechanisms engaged. This is confirmed by our previous X-Ray diffraction studies of evolution of crystalline texture [47] as well as by evolution of the lamellar structure with strain, probed with 2-D SAXS. Fig. 3 compares 2-D SAXS patterns of the virgin and irradiated (200 kGy dose) samples, compressed to selected strains, while Fig. 4 shows the long periods calculated from 1-D sections along LD, FD and CD directions of the 2-D patterns of Fig. 3. Since these patterns do not show point symmetry due to material orientation the Lorentz correction was not applied to the sections and the long period was calculated using Bragg's law directly from the position of the maximum of scattering. It is apparent that all significant transformations of the lamellar structure, producing characteristic changes of scattering patterns and the respective changes in long period [47], occur at the same strain in all samples, irrespective of crosslink density. Kinking of lamellae, producing a 4-point feature in the CD-view pattern occurs around $e = 0.6$, while consequent more extensive lamellae fragmentation, giving rise to a new long period along FD and related 2-point feature emerging in SAXS patterns in both CD- and LD-view, proceeds at $e \geq 1$, which is consistent with the deformation scheme proposed by Strobl [4,15]. For further discussion of evolution of SAXS with strain in the plane-strain compression see Refs. [46,47].

3.3. Strain recovery

In order to study the post-deformation recovery behavior, the samples were deformed to the pre-selected true strain, unloaded, then taken out of the channel-die and left to recover unconstrained at room temperature for a period of time, up to half a year. During the recovery stage, dimensions of the samples were monitored periodically. It was found that the size of the samples along the constrain direction (CD) has not changed with time, which confirms plane-strain state of deformation. On the other hand, sample dimension along LD increased while that along FD decreased during the recovery period. The residual strain, still remaining in the sample, was determined each time from the actual height of the sample (along LD). Fig. 5 illustrates strain recovery behavior of the virgin sample H-0 recovered at room temperature. Irradiated samples recovered at room temperature demonstrated similar behavior. In Fig. 5a, the residual strain, remaining in the sample after indicated period of time is plotted as a function of the true strain applied. Fig. 5b presents the recovered strain component, calculated as a difference between the applied true strain (strain under load) and the residual strain.

Observations of the strain recovery revealed two components of the recovering strain: the fast process, characterized by short and very short relaxation times, observed immediately after unloading and saturating quickly after (in few minutes), and the slow process, relatively intense within first few hours of the recovery period, then slowing down and ceasing in months. The fast recovery process consists of elastic response of the crystalline skeleton and short range interactions within molecular network of the amorphous component. The long relaxation times characteristic for the second, slow process are related to long range interactions within molecular network [10]. That quasi-elastic recovery process is driven by entropic forces in the molecular network of amorphous interlamellar layers that are constrained by neighboring plastically deformed crystals.

Fig. 5b shows that the fast recovery component, represented by the recovered strains measured in samples immediately after unloading, initially increases with an increasing applied strain, then stabilizes around $e = 0.5$ and remains practically constant in a broad range of intermediary strain, up to approximately $e = 1.5$. An amount of the recovered strain in this range is below $\Delta e = 0.2$. At high applied strains, $e > 1.75$, the fast recovery component tends to decrease with an advancing strain. The slow recovery component (illustrated by the recovered strain estimated for lapsed times between 24 h and 6 months after unloading) shows in turn a maximum around an applied strain of $e = 1.0$; at the maximum this component is apparently larger than the fast recovery component, yet diminishes slowly with an increase of strain and finally almost disappears at the strains above of $e = 1.75$. It is worth to note that we observed a very similar recovery behavior also in other grades of polyethylene homo- and copolymers covering a broad range of molecular mass, chain architecture (linear, branched with both short or long branches) and crystallinity [15]. It should be also noticed that the maximum in the slow recovery strain component located at approx. $e = 1$ coincides well with severe destruction of lamellar structure (fragmentation) frequently observed experimentally in compression [47] (see also SAXS patterns of Fig. 3) and the point D of the Strobl's deformation scheme, ascribed to the beginning of chain disentanglement [4]. Then, a decrease of recovered strain observed at higher strains can be interpreted as a result of network deterioration [4,15], related to releasing some of constraints at interfaces due to lamella fragmentation and to molecular network disintegration by either chain disentanglement (as proposed in the Strobl's scheme) or chain scission.

The strain that seems to remain stable at room temperature even after long storage is not truly permanent, since it can be recovered more by rising temperature. Fig. 6 compares recovery behavior of neat and irradiated samples recovered at room temperature (a), then at elevated temperatures of 123 °C, which is slightly below the onset of melting of the crystalline phase (b), and finally at 145 °C, i.e. above the melting temperature (c). It appears that when the sample is heated above the temperature of α relaxation, although still below the melting point (T = 110–123 °C), then it is able to recover an additional strain. The dependence of residual strain on applied strain at elevated temperatures is similar to that observed at room temperature and only an amount of the recovered strain $\Delta e = e - e_r$ increases: from Δe_{max} ~0.4 at room temperature to Δe_{max} ~0.6–0.7 at 110 °C and Δe_{max} ~0.7–0.8 at 123 °C. The maximum of strain recovery is observed at the same strain of

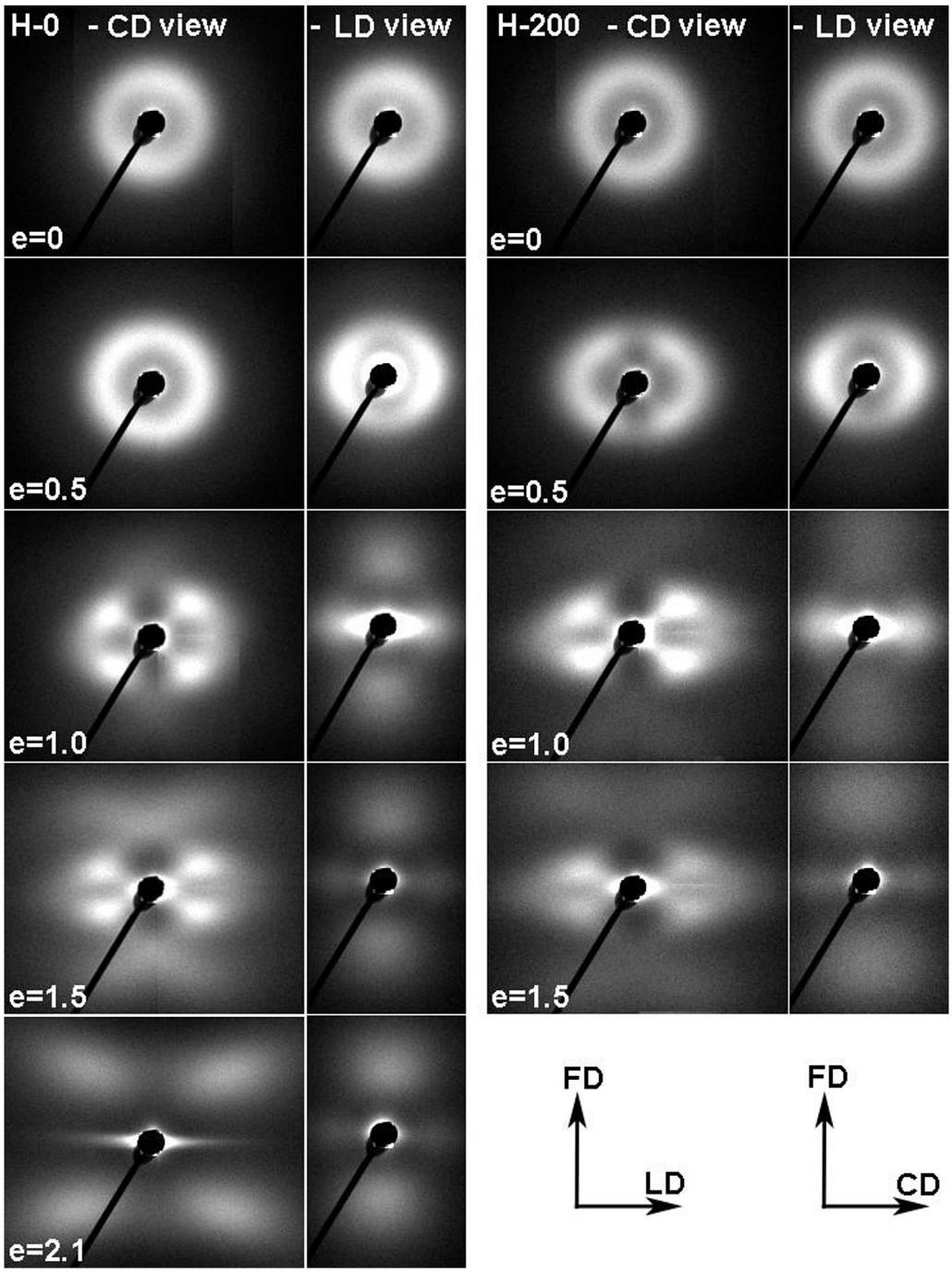

Fig. 3. 2-D SAXS patterns obtained for virgin sample H-0 (not cross-linked; left panel) and cross-linked H-200 (200 kGy dose; right panel), compressed to the true strain indicated. For every sample two pattern are presented: sample illuminated along the CD or LD directions. The flow direction, FD, is vertical in all patterns.

e = 1, regardless of temperature. All this indicates that it is the amorphous component that can recover additional part of the strain, due to activation of α relaxation process and possibly a partial release of constraints imposed on amorphous layers by adjacent crystallites, while the plastic deformation of crystalline phase remains irreversible.

The recovery of crosslinked samples is always higher than of the neat sample due to more robust network with higher network density and significant fraction of solid chemical crosslinks – *cf.* network density data presented in Table 1. The most characteristic difference between the neat (network of entangled chains) and crosslinked samples is an amount of recovery above e = 1.0: while below the melting point H-0 shows a noticeable decrease of the recovered strain Δe with applied strain, all irradiated samples demonstrate stabilization of recovery and only a slight decrease of Δe with applied strain increasing from e = 1.0 to 2.0. Such decrease of Δe in entangled sample H-0 can be related to strain-induced network deterioration, due to e.g. disentangling chain. In irradiated samples the stable chemical crosslinks stabilize the network, making it much more robust and resistant. Chain entanglements are generally entrapped between chemical crosslinks, therefore cannot be resolved easily during deformation. To change the

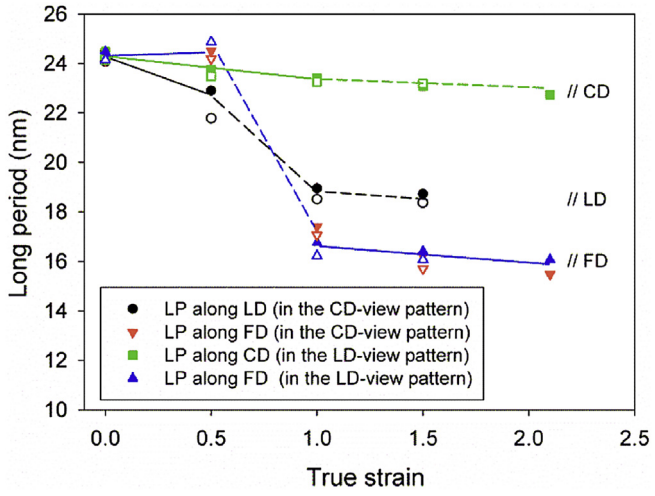

Fig. 4. Long period values along the LD, FD and CD directions, calculated with Bragg's law from one-dimensional sections along respective directions of 2-D SAXS patterns of Fig. 3. The lines do not represent any dependence and are drawn only to guide eye.

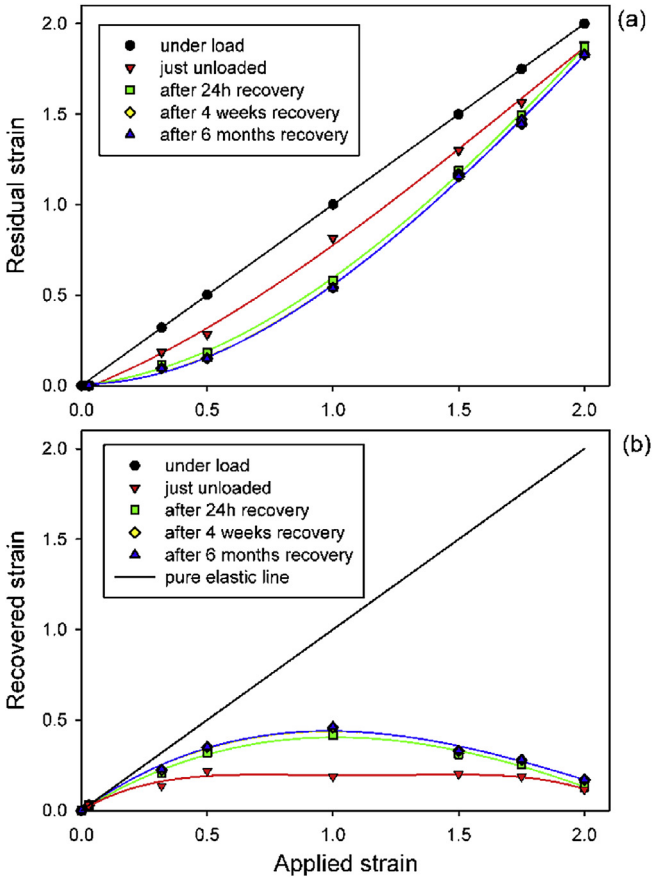

Fig. 5. Residual (a) and recovered (b) strain components determined for sample of neat HDPE (H-0) deformed and recovered at room temperature. Note, that the curves for recovery periods of 4 weeks and 6 months run very close each to the other.

properties of such network breaking of numerous chemical bonds would have to occur. In the case of both neat and crosslinked materials, a partial destruction of the crystalline phase during deformation, relieving some of the constraints, can also contribute to the decrease of recovery at high strain.

The recovery behavior changes noticeably after melting of

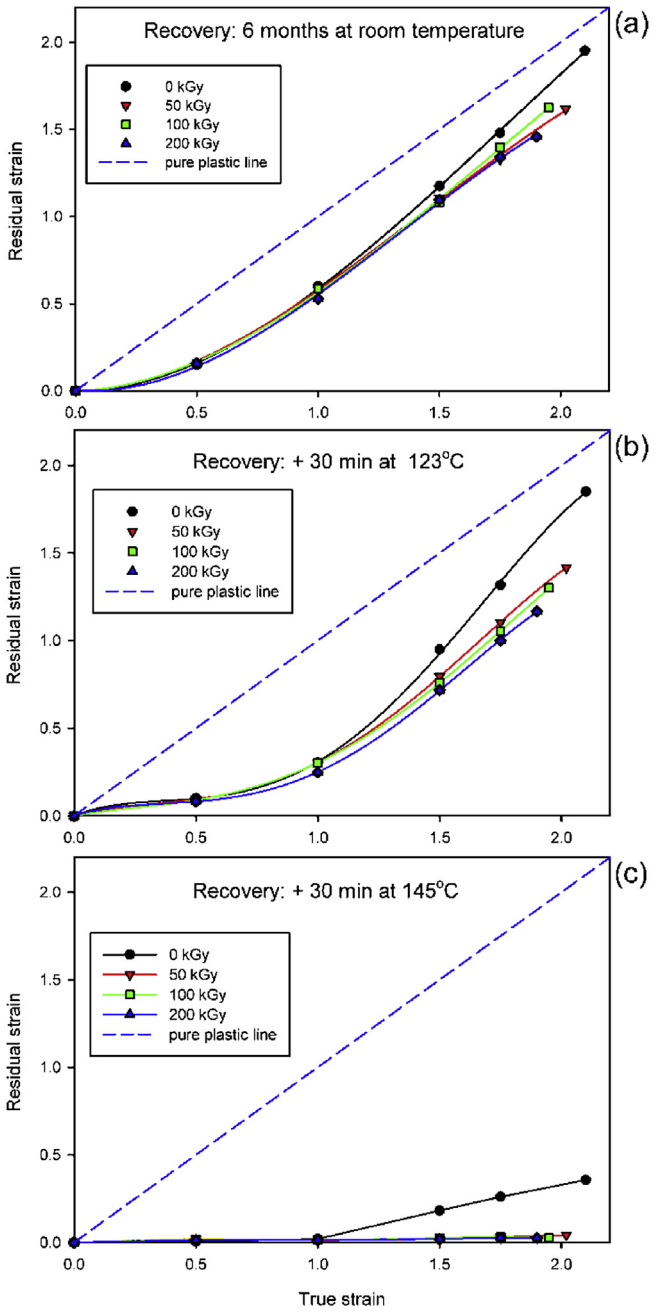

Fig. 6. The dependence of the residual strain on applied strain for PE samples of different crosslinking degree: (a) room temperature, measured 6 months after unloading; (b) after annealing at 123 °C by 30 min; (c) after further annealing at 145 °C by 30 min.

crystallites upon annealing at 145 °C, which causes release of all constraints imposed earlier on amorphous component by adjacent irreversibly deformed crystals. Then, in absence of constraints, the recovery process driven by entropic forces in the molecular network of the molten sample can progress further – *cf.* Fig. 6c demonstrating that for applied strain lower than e = 1, practically all applied strain was recovered at T = 145 °C, irrespectively of sample topology (entangled or crosslinked). Above e = 1 the crosslinked samples were still able to recover fully (the observed residual strain $e_{res} < 0.02$ is well below the limit of experimental error) while in the sample H-0, containing only entangled chains, a fraction of the strain appeared irreversible. This finite residual

strain, which can be considered as truly permanent, rises from $e_r = 0$ at $e = 1$ to approx. 0.35 at $e = 2.1$. This behavior confirms suggestions given earlier – networks of crosslinked chains survived the deformation even to high strain approaching $e = 1.5–2$ ($\lambda = 4.5–7.4$) most probably unaltered, while the network of entangled chains had to be partially destroyed, which resulted in an increasing permanent flow upon deformation and a non-reversible, permanent residual strain left in the material.

3.4. Changes in molecular network due to deformation

The molecular weight and its distribution were monitored in non-crosslinked samples after their deformation in a broad range of applied strain. Fig. 7a presents the obtained chromatographs, while Fig. 7b the determined weight- and number averaged molecular mass of investigated samples. Both figures demonstrate clearly that there is no significant difference in molecular weight and its distribution between initial and all deformed samples, therefore no influence of the strain history on the length of chains. The small statistical variation in M_n or M_w, observed in Fig. 7b, does not exceed the limit of experimental error. On this basis, the chain scission can be excluded as a mechanism contributing significantly to the deterioration of the molecular network.

The irradiated samples, insoluble due to crosslinking, could not be analyzed with GPC. Instead, the state of the network in such samples subjected to heavy deformation was evaluated on the basis of extraction and swelling experiments. The results of estimations are presented in Table 2. They demonstrate that a high-strain deformation ($e = 1.75$) of crosslinked samples practically does not lead to any change of the network properties: both the insoluble gel content and crosslink density remain nearly unaltered after deformation (a small reduction of gel content as well as small increase of the crosslink density are actually within the limit of experimental error). This observation allows to conclude that the network in crosslinked samples survives unaltered even a heavy deformation.

The results of calorimetric studies of deformed samples, presented in Table 3, demonstrate a small decrease of crystallinity in samples deformed to $e = 1.75$ as compared to undeformed samples, similar for all samples, irrespective of the crosslink density. Concurrently, the onset temperature of melting increases in all samples, while the peak temperature increases in neat H-0 and decreases in irradiated H-50 - H-200 samples after their deformation. Assuming the existence of a mechanism generating chain scissions, a chemicrystallization phenomenon should have been observed, resulting in an increase in both X_c and T_m [52], which is apparently not the case here. The observed changes in crystallinity and melting behavior support rather the view of deformation-induced destruction of the lamellar structure: fragmentation of lamellae in H-0 as a result of an advanced crystallographic slip, that occurs preferentially at points of the smallest thickness of lamellae [46,47]. That fragmentation involves a local destruction of the thinnest parts of lamellar crystals, hence a decrease of X_c and increase of T_{ons} and T_m are expected. Fragmentation begins at e ~1.0, in addition to partial disintegration of the molecular network within amorphous layers, as indicated by results presented above. On the other hand, an increase of T_{ons} and reduction of T_m, observed in irradiated samples suggests that not only the thinnest (melting at T_{ons}) but also a fraction of thick lamellae (T_m) had to be destroyed in these samples. Such a behavior can be read as a mark of a competition between network and crystal damage – in crosslinked samples destruction of crystals apparently appears easier than disintegration of the network of crosslinked chains within amorphous phase, what is opposite to entangled samples, in which partial destruction of the molecular network erosion seems easier than crystal damage.

More information about the possible network damage due to chain scission mechanism can be obtained from FTiR spectroscopy, which is a very sensible tool able to detect even very small changes in the chemical structure of the material. Polyethylene undergoes chain scission by breaking of the carbon-carbon bonds along its backbone, leading to the formation of terminal methyl, vinyl and/or carbonyl groups if oxygen is present [53]. The number of chain scissions accompanying deformation can be then estimated from i.R. analysis of concentration of new end groups appearing in deformed samples. The FTiR measurements were performed after the half a year recovery period, which was long enough to complete all reactions, possibly triggered by deformation.

Comparison of the spectra of the deformed samples of non-crosslinked polymer (H-0-e) with that of the virgin sample H-0-0 (Fig. 8) revealed no difference in bands associated with end methyl groups (1378 cm^{-1}) or methylene groups (1142 cm^{-1}, 1310 cm^{-1}, 1368 cm^{-1}). There were also no deformation-related changes in the region of 900–1000 cm^{-1}, where the bands of terminal vinyl groups (909 cm^{-1}, 990 cm^{-1}) are observed (*cf.* Fig. 8b), consistently with the stability of another band, at 1642 cm^{-1}, related to vibration of the double bond in the vinyl group (*cf.* Fig. 8a). The 965 cm^{-1} band, characteristic for *trans*-vinylene structure, which could originate from branching and/or crosslinking [32], is absent in the virgin as well as in all deformed

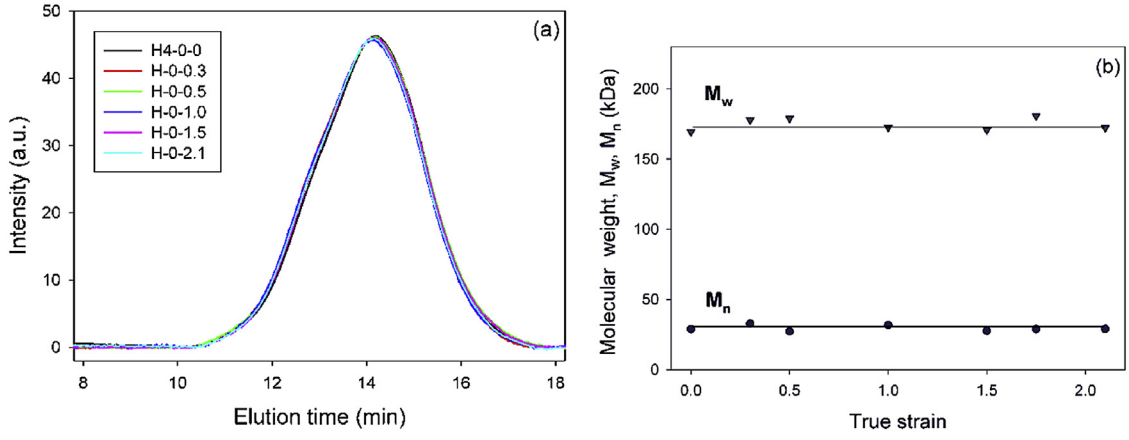

Fig. 7. The high temperature GPC chromatographs of H-0 samples (not crosslinked HDPE) subjected to deformation to the true strain of $e = 0.3–2.1$ (a); and the average molecular mass M_w (∇) and M_n (•), derived from these curves (b).

Table 2
Gel content, swell ratio, average molecular weight between chemical crosslinks and the cross-link density calculated for raw and deformed specimens of PE samples irradiated with the absorbed dose of 50 and 200 kGy.

Sample	Applied true strain	Gel content, (wt.%) [a]	M_c (g/mol) [b]	$N_x \times 10^{-26}$ (1/m^3) [c]
H-50-0	0	59.1	5930	0.82
H-50-1.75	1.75	58.5	5470	0.89
H-200	0	76.6	1840	2.63
H-200-1.75	1.75	75.8	1710	2.84

[a] Calculated with Eq. (2).
[b] Calculated with Eqs. (2)–(5).
[c] Calculated with Eq. (6).

Table 3
Thermal data of deformed samples (DSC heating scan, 10 °C/min).

Sample	True strain	T_{ons} (°C)	T_m (°C)	X_c (wt.%)
H-0-0	0	125.6	134.1	71.5
H-0-1.75	1.75	130.2	135.7	67.8
H-50	0	124.3	134.4	70.7
H-50-1.75	1.75	129.2	133.2	66.0
H-100	0	124.5	134.6	71.3
H-100-1.75	1.75	127.8	132.3	66.3
H-200	0	123.6	134.1	69.2
H-200-1.75	1.75	127.9	131.2	63.9

samples. The above observations indicate clearly that no new terminal methyl or vinyl groups were formed at any stage of the deformation process. Branching or crosslinking, following chain rupture, can be also excluded. Moreover, analysis of spectra in the range above 3000 cm^{-1} did not reveal development of hydroperoxide or hydroxyl bands during deformation.

In contrast to methylene and vinyl ranges, the carbonyl region of spectra shows some changes of the carbonyl bands range between 1750 and 1690 cm^{-1} with increasing strain (see Fig. 8b). The bands at 1750-30 cm^{-1}, 1714 cm^{-1} and 1698 cm^{-1} were analyzed quantitatively. The intensity of these bands appeared to remain roughly constant up to the true strain of e = 1.0 and then increased slowly with further strain increase. In the literature the bands at 1750-30 cm^{-1}, 1714 cm^{-1} and 1698 cm^{-1} in the mechano-oxidative degraded samples have been attributed to aldehydes/esters, ketones/acids and unsaturated ketones/esters, respectively [26–28]. Costa et al. [32] identified that mechano-oxidation gives rise primarily to the formation of acid (1714 cm^{-1}) and ester groups (1741 cm^{-1}). From the integral absorbance data determined for the discussed bands the concentrations of carbonyl groups were calculated using the Lambert's law with the respective integral molar extinction coefficients listed in Experimental section. The total concentration of carbonyl groups was approximated by the sum of the determined concentrations of ester/aldehydes, acids and unsaturated ketone groups. The results are presented in Fig. 9.

It can be seen that the concentration of all analyzed carbonyl groups at low and moderate strain, up to the true strain of e = 1, remains practically constant, and then, for e > 1, become to rise slowly with an advancing strain. This dependence resembles very much the residual strain dependence observed in the strain recovery behavior (*cf.* Fig. 6c), with the same cross-over point around the true strain of e = 1. Therefore, it can be inferred that chain scission that probably leads to formation of end carbonyl groups, detected in heavily deformed samples, may contribute to erosion of the molecular network, manifesting in truly irreversible strain, generated above e = 1. On the other hand, the estimated concentration of carbonyl group remains very low in the entire range of strain – it varies from 0.12 to 0.20 mmol/kg. Assuming that all new carbonyls are related to chain scission products and no crosslinking phenomena occurred, the corresponding changes in molecular weight can be calculated with the following equations [54]:

$$\frac{1}{M_n} - \frac{1}{M_{n0}} = c_s \tag{7a}$$

$$\frac{1}{M_w} - \frac{1}{M_{w0}} = \frac{c_s}{2} \tag{7b}$$

where M_{n0} and M_{w0} are initial number- and weight average molecular mass, and c_s is the concentration of chain scission, here assumed equal to the concentration increment of carbonyl groups. Calculations based on the above equations demonstrate that the

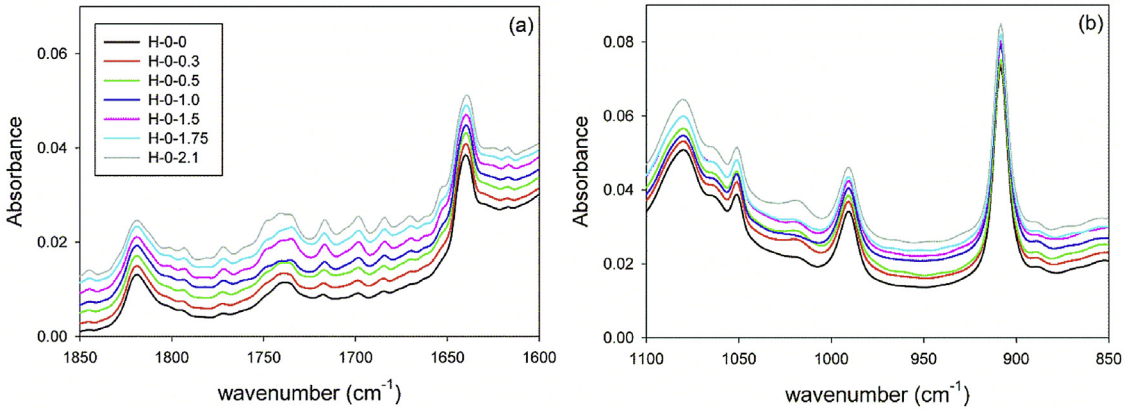

Fig. 8. FTiR spectra of non-crosslinked samples of HDPE prior to deformation and deformed to various true strains, indicated. (a) the region of carbonyl bands; (b) the region of vinyl bands. All spectra were normalized at the 2020 cm^{-1} peak and shifted vertically by a factor of 0.001 for clarity of presentation.

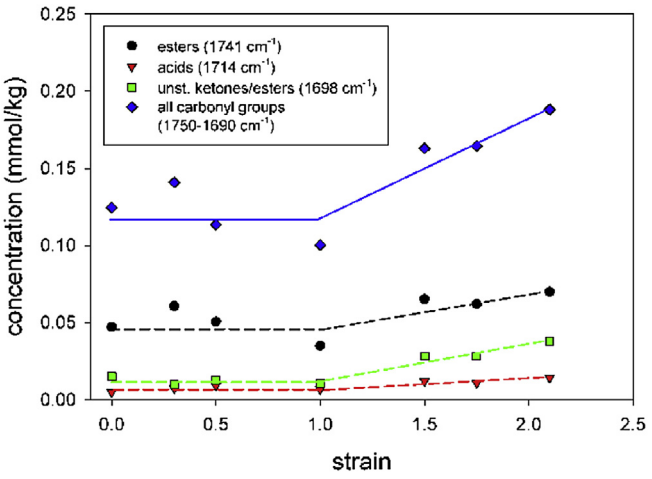

Fig. 9. Concentration of carbonyl groups in deformed samples of non-crosslined HDPE (H-0 series) as a function of the applied true strain. The lines are drawn only to guide eye.

change of molecular mass corresponding to chain scission in deformed samples is negligibly small: for the high strain e = 2.1 the calculated ratio M_n/M_{no} = 0.998 while M_w/M_{wo} = 0.993. This estimation is in line with GPC results presented in Fig. 7, which indicate practically no change in molecular mass in deformed samples.

The range of carbonyl concentration reported above corresponds to merely 0.0018–0.0030 carbonyl group per 1000 CH_2 units. From here, the concentration increment calculated per average chain (M_n = 28,900) is well below 0.002 that means merely one new carbonyl group appearing per more than 500 average chains in highly deformed samples, which corresponds to scission of less than one of 1000 chains (breaking of a single chain leads to creation of two new end groups). Taking into account that an average chain statistically contributes to the molecular network of entangled chains through about 20 entanglements, the number of detected scissions seems much too small to account for observed permanent residual strain (e_r = 0.35 at e = 2.1) resulting from gradual disintegration of the molecular network, allowing plastic flow. It becomes clear that another, much more intense mechanism(s) was necessary to cause an erosion of the network, and consequently enable plastic flow and produce the permanent residual strain. In our opinion, the chain disentanglement (driven by the shear flow leading to chains reptating out of entanglement knots) must be that active mechanism playing the primary role in strain-induced gradual erosion of the network. Such resolving of entanglements can be relatively easy and effective in the case of studied linear polyethylene of moderate average molecular mass and distribution, containing a significant fraction of relatively short chains, easy do disentangle. The flow produced by interlamellar shear is probably large enough to disentangle such short chains and resolve also entanglements of longer chains, located closer to the chain end. It can be envisaged that with increasing molecular weight, the relative contribution of chain disentanglement to erosion of the network may decrease. On the other hand, it seems that the complete resolution of an entanglement is not always required to change the network properties. It is possible that a much easier translation of mobile entanglements along the chain can appear sufficient to modify response of the network.

The other plausible mechanism of network modification can be a partial release of constraints imposed on amorphous layers by adjacent lamellae, induced by their fragmentation. The transition point of the recovery behavior at approx. e = 1 coincides well with severe destruction of lamellar structure by fragmentation, observed in compression [47] (see also SAXS patterns of Fig. 3). This transformation produces small crystalline blocks, loosely connected, that are much more mobile than the long lamellae prior to fragmentation. This new structure can result in release a number of constraints imposed on amorphous phase by lamellae through chains crossing interface, which have played the role of solid physical crosslinks in the molecular network. Thus, it is equivalent to a decrease of an effective crosslink density of the network. Additionally, a fraction of such interface crosslinks simply disappears when some fragments of lamellae at boundaries between blocks are completely destroyed during fragmentation process and become incorporated by an amorphous phase. These mechanisms of reduction of effective crosslink density seem, however, practically insignificant, since they should be equally active in samples with the network of entangled chains and in those with crosslinked chains, both materials undergoing very similar lamellar fragmentation at the same strain range (*cf.* Fig. 3). Therefore, both entangled and crosslinked samples might develop then similar permanent strain due to facilitated plastic flow. However, this is evidently not the case here – a permanent deformation was observed only in entangled samples, while the response of the crosslinked network remained purely elastic up to the highest strain reached, in spite of very similar changes in lamellar morphology upon deformation in both materials. This means that the mechanism of reduction of physical crosslink density due to lamella fragmentation does not play any important role in the process of network erosion.

The FTiR study of samples crosslinked by an electron beam irradiation demonstrated that the chemical structure of irradiated HDPE changed notably due to crosslinking and additionally that the crosslinked material changed its chemical structure slightly more due to heavy deformation (see Fig. 10 presenting exemplary results of the H-200 sample, crosslinked with the absorbed dose of 200 kGy). In the carbonyl region, 1750-1690 cm^{-1}, all bands developed in crosslinked material much higher comparing to neat HDPE, with the acid band at 1714 cm^{-1} becoming the strongest one. The bands associated with end-vinyl groups (1642, 990, 909 cm^{-1}) notably reduced, while the new *trans*-vinylene band at 965 cm^{-1}, absent in the neat polymer, developed in the crosslinked samples. Such changes are typical for polyethylene crosslinked by irradiation [31,55,56].

Concentration of carbonyl, end vinyl and *trans*-vinylene groups was evaluated from integral absorbance of respective bands using the Lambert's law and relevant molar extinction coefficients. The results of these estimations for H-200 series are summarized in Fig. 11. Concentration of terminal vinyls slightly decreases while concentration of *trans*-vinylene slowly increases with increasing strain. In contrast to non-crosslinked samples (H-0, see Fig. 9), concentration of carbonyl groups keeps approximately constant up to e = 1.5 and then seems to increase in sample deformed to e = 1.9. Unfortunately, the H-200 material fractured usually at strains above e = 1.5, and the specimen of e = 1.9 used in this experiment was partially fractured, what could lead to an excessive number of carbonyls detected, as fracture phenomena could involve some chain scission. Therefore, the value of carbonyl concentration determined for this particular sample is less reliable than others. On the other hand, the contribution of esters, acids and unsaturated ketone/esters to the carbonyl region 1750-1690 cm^{-1} was generally similar in all crosslinked samples, which can support the view that there was no stress induced chain scissions [56]. The above observations indicate that the network of crosslinked chains was not damaged by a heavy deformation.

Summarizing, we can conclude that two plausible mechanisms of network erosion, by (i) chain scission or (ii) elimination of a fraction of physical crosslinks at crystal-amorphous interface due to

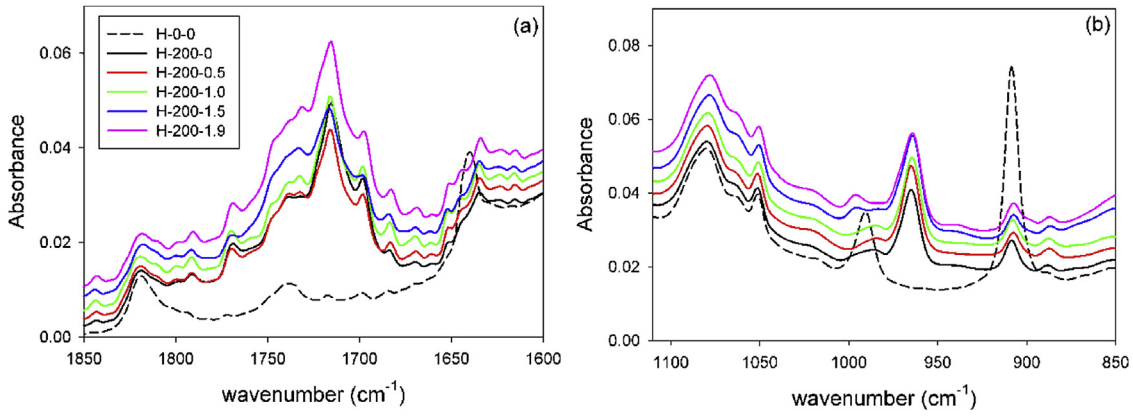

Fig. 10. FTIR spectra of HDPE samples crosslinked with the dose of 200 kGy (H-200 series), prior to deformation and deformed to various true strains, indicated. (a) the range of carbonyl bands; (b) the range of vinyl bands. Spectra were normalized at 2020 cm^{-1} and shifted vertically for clarity of presentation. For comparison the spectrum of the neat undeformed sample H-0-0 is also shown.

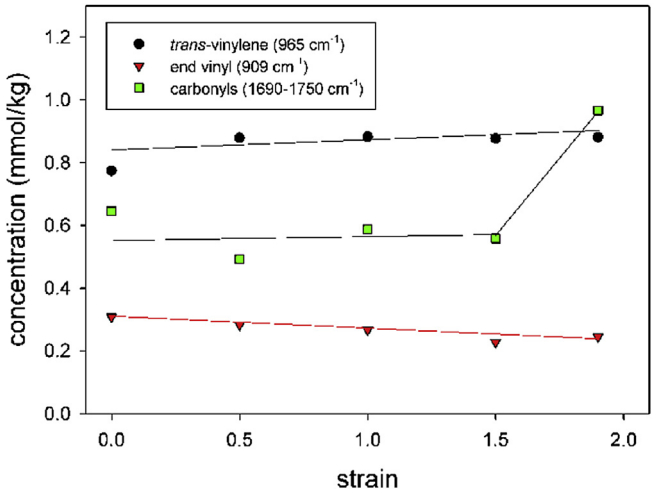

Fig. 11. Concentration of carbonyl, vinyl and *trans*-vinylene groups estimated for samples of crosslinked and deformed HDPE (H-200 series) as a function of the applied true strain. The lines are drawn only to guide eye.

partial destruction of the lamellar structure, demonstrated both very limited activity. This undoubtedly means that the primary mechanism of network erosion must be the chain disentanglement, discussed above.

Our experimental findings concerning various activity of chain disentanglement with strain agree quite well with the predictions of recent model calculations performed by Billon et al. [34,35] who developed the model (Visco Elastic Network Unit, VENU), based on the Edward -Vilgis slip-link theory [57] and accounting for network reorganization under external loading through mobility of entanglement points. The model accounts for solid crosslinks as well as entanglements and their evolution as a function of strain energy: weak entanglements are initially not mechanically active and act as crosslinks at low stress/strain, then gain a certain level of mobility as a function of strain energy, which induces visco-elasticity and finally, with further increase of strain energy, entanglements gain even more in mobility, which corresponds to disentanglement and visco-plasticity. That behavior of the network of entangled chains in a deformed semicrystalline polymer is basically the same as that found experimentally and described in this study.

All the results discussed in this paper refer to polymer response to deformation in the plane-strain compression mode, in which the plastic deformation is not accompanied and obscured by any side-effects, as e.g. cavitation, which is inhibited by compressive stress components generated in the material. However, the situation may be markedly different in other deformation modes, especially those accompanied by a widespread cavitation, like e.g. uniaxial tension. The particular stress distribution in tensile deformation mode facilitates cavitation that often begins even before reaching the macroscopic yield point [58]. Formation of a cavity is a local event of micro-fracture and is highly probable that chain scission contributes significantly to the formation of new polymer-cavity interfaces. Therefore, the contribution of chain scission to modification of the molecular network during tensile deformation can be notably larger than a small share observed by us in compression. Moreover, since cavitation starts at early stages of deformation, the accompanying chain scission may result in noticeable deterioration of the molecular network much earlier than that taking place in compression due to chain disentanglement, commencing above the true strain of $e = 1$.

On the other hand, the stress distribution in tension and ongoing cavitation releasing some of local constraints allow lamellae fragmentation much easier than in compression. This eventually leads to fast completion of transformation of the initial structure into a new micro-fibrillar structure. That nearly unconstrained transformation is accompanied by a strong orientation and flow of neighboring amorphous material that facilitates chain disentanglement and more chain scission, both leading to partial destruction of the molecular network and irreversible flow, which may be even stronger than these observed in compression.

4. Conclusions

The long-term recovery and the recovery at elevated temperature, above the melting point of crystalline phase of highly deformed polyethylene revealed that a significant part of the applied strain appeared reversible due to rubber-like elasticity of the molecular network within amorphous phase.

At the true strain increasing to $e = 1.0$ the strain component recovered after unloading at room temperature also increases and approaches the value of 0.5, irrespective of degree of crosslinking of the amorphous phase, and then tends to decrease with further strain increase above 1.0. In contrast, the recovery at temperature above the melting point (when all constraints imposed earlier on amorphous phase by adjacent crystals disappear) depends only on

the presence of chemical crosslinks in amorphous phase: crosslinked samples are able to recover practically all strain, even for the highest applied strains, while the non-crosslinked samples, in which amorphous phase constitutes primarily a molecular network of entangled chains, recover fully only for applied true strains below e = 1.0 and demonstrate a permanent non-reversible residual strain component that rises gradually from 0 to 0.36 for applied strain increasing from 1.0 to 2.1.

The change of the recovery behavior around e = 1.0 is related to stress built-up during deformation, due to straining of the molecular network within amorphous phase. Moreover, at strain around e = 1.0 the lamellae already thinned significantly by an advanced chain slip undergo partial destruction through fragmentation into smaller blocks due to that increase of the stress, non-uniform lamella thickness and additionally local stress concentrations developing at interfaces, related to e.g. tie-molecules becoming fully stretched. This partial destruction of lamellar structure relieves some of constraints imposed earlier on amorphous layers by adjacent crystals, which facilitates further deformation of the molecular network, leading eventually to a strong strain hardening of amorphous phase that gradually approaches its extensibility limit. High strain and related high stress induce erosion (partial destruction) of the molecular network, primarily through chain disentanglements, in the neat, not crosslinked HDPE. This in turn results in increasing irreversible flow and reduction of the strain recoverable at temperatures below the melting point. A significant part of the residual strain appears truly permanent as it does not recover even after melting of the crystalline component, which releases all previous constraints imposed on amorphous phase.

In irradiated samples, in which the molecular network of amorphous phase is stabilized by strong chemical cross-links the advanced deformation is not able to destroy or alter that network −the deformation of irradiated samples appears 100% reversible after melting of crystals (complete recovery). High strains generating very high stress lead to a competition between network and crystal damage. The partial destruction of crystals appears easier than destruction of the chemical bonds of crosslinked network of amorphous phase. Consequently a reduction of crystallinity of deformed irradiated samples was observed.

From the identified mechanisms of network erosion the chain disentanglement appears the primary mechanism. It is supported by a limited chain scission, which plays only a secondary role. The third plausible mechanism − elimination of a fraction of physical crosslinks at crystal-amorphous interface by partial destruction of the lamellar structure does not seem to have any practical influence on the state of the network and consequently an ability of the material to recover strain. The erosion of the network occurs only when the deformation is well advanced - at high strain above e = 1.0, since large local strains are needed for chain disentanglement. What is important, such strain can develop in amorphous layers only after destruction of the initial lamellar structure, which initially constrains strongly amorphous layers and does not allow for high deformation within these layers.

The reported study concerns deformation by plane-strain compression. However, an evolution of the molecular network can take place in a different way when a polymer is deformed in other deformation modes, facilitating cavitation, as e.g. tension, since chain scission, presumably accompanying cavitation, can contribute to disintegration of the molecular network significantly more than in compression, where it appeared merely a secondary mechanism. Moreover, cavitation and perhaps the related chain scission set in already at low strain, near the macroscopic yield point. Therefore, a partial destruction of the network, and consequently an irreversible plastic flow may develop in tensile samples at strains lower than in those subjected to compression.

Acknowledgement

This project was financed from the funds of the National Science Centre, Poland, on the basis of the decision number DEC-2014/15/B/ST8/04306.

Authors gratefully acknowledge the Carnot-Arts Institute for its financial support to acquire an Agilent Technologies PL-GPC 220 high temperature device (project CEQUAM).

References

[1] E.F. Oleinik, Plasticity of semicrystalline flexible-chain polymers at the microscopic and mesoscopic levels, Polym. Sci. C 45 (1) (2003) 17−117.
[2] Z. Bartczak, A. Galeski, Plasticity of semicrystalline polymers, Macromol. Symp. 294 (1) (2010) 67−90.
[3] Z. Bartczak, M. Kozanecki, Influence of molecular parameters on high-strain deformation of polyethylene in the plane-strain compression. Part I. stress-strain behaviour, Polymer 46 (2005) 8210−8221.
[4] R. Hiss, S. Hobeika, C. Lynn, G. Strobl, Network stretching, slip processes, and fragmentation of crystallites during uniaxial drawing of polyethylene and related copolymers. A comparative study, Macromolecules 32 (1999) 4390−4403.
[5] S. Hobeika, Y. Men, G. Strobl, Temperature and strain rate independence of critical strains in polyethylene and poly(ethylene-co-vinyl acetate), Macromolecules 33 (5) (2000) 1827−1833.
[6] Y. Men, J. Riegel, G. Strobl, Role of the entangled amorphous network in tensile deformation of semicrystalline polymers, Phys. Rev. Lett. 91 (9) (2003) 955021−955024.
[7] B.J. Lee, A.S. Argon, D.M. Parks, S. Ahzi, Z. Bartczak, Simulation of large-strain plastic-deformation and texture evolution in high-density polyethylene, Polymer 34 (17) (1993) 3555−3575.
[8] A. Peterlin, Molecular model of drawing polyethylene and polypropylene, J. Mater. Sci. 6 (1971) 490−508.
[9] B. Xiong, O. Lame, J.-M. Chenal, C. Rochas, R. Seguela, On the strain-induced fibrillar microstructure of polyethylene: influence of chemical structure, initial morphology and draw temperature, eXPRESS Polym. Lett. 10 (4) (2016) 311−323.
[10] Z. Bartczak, Effect of the molecular network on high-strain compression of cross-linked polyethylene, Eur. Polym. J. 48 (12) (2012) 2019−2030.
[11] H.E.H. Meijer, L.E. Govaert, Mechanical performance of polymer systems: the relation between structure and properties, Prog. Polym. Sci. 30 (2005) 915−938.
[12] R.N. Haward, G. Thackray, Use of a mathematical model to describe isothermal stress-strain curves in glassy thermoplastics, Proc. R. Soc. Lond. Ser. A 302 (1967) 453−472.
[13] H.G.H. van Melick, L.E. Govaert, H.E.H. Meijer, On the Oorigin of Sstrain Hhardening in Gglassy Ppolymers, Polymervol 44 (2003) 2493−2502.
[14] R.G.C. Arridge, P.J. Barham, A. Keller, Self-hardening of highly oriented polyethylene, J. Polym. Sci. Polym. Phys. Ed. 15 (1977) 389−401.
[15] Z. Bartczak, Influence of molecular parameters on high-strain deformation of polyethylene in the plane-strain compression. Part II. Strain recovery, Polymer 46 (23) (2005) 10339−10354.
[16] K. Hong, A. Rastogi, G. Strobl, A model treating tensile deformation of semicrystalline polymers: quasi-static Stress−Strain relationship and viscous stress determined for a sample of polyethylene, Macromolecules 37 (26) (2004) 10165−10173.
[17] K. Hong, G. Strobl, Network stretching during tensile drawing of polyethylene: a study using X-ray scattering and microscopy, Macromolecules 39 (2006) 268−273.
[18] L. Treloar, The Physics of Rubber Elasticity, Clarendon Press, Oxford, 1975.
[19] Z. Bartczak, Effect of chain entanglements on plastic deformation behavior of linear polyethylene, Macromolecules 38 (2005) 7702−7713.
[20] Z. Bartczak, Effect of chain entanglements on plastic deformation behavior of ultra-high molecular weight polyethylene, J. Polym. Sci. Part B Polym. Phys. 48 (3) (2010) 276−285.
[21] H.H. Kausch, Polymer Fracture, Springer Verlag, Berlin, Heidelberg, 1978.
[22] A.J. Kinloch, R.J. Young, Fracture Behaviour of Polymers, Applied Science Publishers, London, 1983.
[23] A. Casale, R.S. Porter, J. Johnson, The mechanochemistry of high polymers, Rubber Chem. Technol. 44 (1971) 534−577.
[24] T.M. Stoeckel, J. Blasius, B. Crist, Chain rupture and tensile deformation of polymers, J. Polym. Sci. Polym. Phys. Ed. 16 (1978) 485−500.
[25] R.P. Wool, A.T. Rockhill, Molecular fracture in polystyrene, J. Macromol. Sci. B20 (1981) 85−99.
[26] S.N. Zhurkov, V.E. Korsukov, Atomic mechanism of fracture of solid polymers, J. Polym. Sci. Polym. Phys. Ed. 12 (1974) 385−398.
[27] B.M. Fanconi, Chain scission and mechanical failure of polyethylene, J. Appl. Phys. 54 (10) (1983) 5577.
[28] B.M. Fanconi, K.L. DeVries, R.H. Smith, Free-radicals and new end groups resulting from chain scission .2. Mechanical degradation of polyethylene, Polymer 23 (7) (1982) 1027−1033.

[29] A. Sedighiamiri, L.E. Govaert, M.J.W. Kanters, J.A.W. van Dommelen, Micro-mechanics of semicrystalline polymers: yield kinetics and long-term failure, J. Polym. Sci. Part B Polym. Phys. 50 (24) (2012) 1664–1679.
[30] U.W. Gedde, J. Viebke, H. Leijström, M. Ifwarson, Long-term properties of hot-water polyolefin pipes—a review, Polym. Eng. Sci. 34 (24) (1994) 1773–1787.
[31] K. Czaja, M. Sudoł, Studies on electron-beam irradiation and plastic deformation of medical-grade ultra-high molecular weight polyethylene, Radiat. Phys. Chem. 80 (3) (2011) 514–521.
[32] L. Costa, M.P. Luda, L. Trossarelli, Ultra-high molecular weight polyethylene .1. Mechano-oxidative degradation, Polym. Degrad. Stab. 55 (3) (1997) 329–338.
[33] J.L. Bouvard, D.K. Ward, D. Hossain, S. Nouranian, E.B. Marin, M.F. Horstemeyer, Review of hierarchical multiscale modeling to describe the mechanical behavior of amorphous polymers, J. Eng. Mater Technol. 131 (4) (2009) 041206.
[34] A. Maurel-Pantel, E. Baquet, J. Bikard, J.L. Bouvard, N. Billon, A thermo-mechanical large deformation constitutive model for polymers based on material network description: application to a semi-crystalline polyamide 66, Int. J. Plasticity 67 (2015) 102–126.
[35] N. Billon, Time dependent mechanical modeling for polymers based on network theory, AIP Conf. Proc. 1736 (2016) 020088, http://dx.doi.org/10.1063/1.4949663.
[36] B. Wunderlich, G. Czornyj, A study of equilibrium melting of polyethylene, Macromolecules 10 (1977) 906–913.
[37] P.J. Flory, Principles of Polymer Chemistry, Cornell Unversity Press, New York, 1953.
[38] P.J. Hendra, A.J. Peacock, H.A. Willis, The morphology of linear polyethylenes crosslinked in their melts. The structure of melt crystallized polymers in general, Polymer 28 (1987) 705–709.
[39] Z. Hrnjak-Murgic, J. Jelencic, M. Bravar, M. Marovic, Influence of the network on the interaction parameter in system EPDM vulcanizate-solvent, J. Appl. Polym. Sci. 65 (1997) 991–999.
[40] A. Solti, D.O. Hummel, P. Simak, Computer-supported infrared spectrometry of polyethylene, ethene copolymers, and amorphous poly(alkyl ethylene)s, Makromol. Chem. Macromol. Symp. 5 (1) (1986) 105–133.
[41] K. Jacobson, L. Costa, P. Bracco, N. Augustsson, B. Stenberg, Effects of microtoming on oxidation of ultra high molecular weight polyethylene (UHMWPE), Polym. Degrad. Stab. 73 (1) (2001) 141–150.
[42] J.F. Rabek, Polymer Photodegradation: Mechanisms and Experimental Methods, in: Ch.10 Experimental Methods in Polymer Degradation, Chapman & Hall, London, 1995, pp. 505–515.
[43] J. Fu, B.W. Ghali, A.J. Lozynsky, E. Oral, O.K. Muratoglu, Wear resistant UHMWPE with high toughness by high temperature melting and subsequent radiation cross-linking, Polymer 52 (4) (2011) 1155–1162.
[44] D.S. Pearson, L. F, W.W. Graessley, G. Ver Strate, E. von Meerwall, Viscosity and self-diffusion coefficient of hydrogenated polybutadiene, Macromolecules 27 (1994) 711–719.
[45] C. G'Sell, J.M. Hiver, A. Dahoun, A. Souahi, Video-controlled tensile testing of polymers and metals beyond the necking point, J. Mater. Sci. 27 (1992) 5031–5039.
[46] A. Galeski, Z. Bartczak, A.S. Argon, R.E. Cohen, Morphological alterations during texture-producing plastic plane strain compression of high-density polyethylene, Macromolecules 25 (1992) 5705–5718.
[47] Z. Bartczak, E. Lezak, Evolution of lamellar orientation and crystalline texture of various polyethylenes and ethylene-based copolymers in plane- strain compression, Polymer 46 (16) (2005) 6050–6063.
[48] N.W.J. Brooks, M. Mukhtar, Temperature and stem length dependence of the yield stress of polyethylene, Polymer 41 (2000) 1475–1480.
[49] K. Jordens, G.L. W, J. Janzen, D.C. Rohlfing, M.B. Welch, The influence of molecular weight and thermal history on the thermal, rheological, and mechanical properties of metallocene-catalyzed linear polyethylenes, Polymer 41 (2000) 7125–7192.
[50] S. Humbert, O. Lame, G. Vigier, Polyethylene yielding behaviour: what is behind the correlation between yield stress and crystallinity? Polymer 50 (2009) 3755–3761.
[51] A. Menyhard, P. Suba, Z. Laszlo, H.M. Fekete, A.O. Mester, Z. Horvath, et al., Direct correlation between modulus and the crystalline structure in isotactic polypropylene, eXPRESS Polym. Lett. 9 (3) (2015) 308–320.
[52] B. Fayolle, E. Richaud, X. Colin, J. Verdu, Review: degradation-induced embrittlement in semi-crystalline polymers having their amorphous phase in rubbery state, J. Mater Sci. 43 (22) (2008) 6999–7012.
[53] M.L. Poutsma, Reexamination of the pyrolysis of Polyethylene: data needs, free-radical mechanistic considerations, and thermochemical kinetic simulation of initial product-forming pathways, Macromolecules 36 (2003) 8931–8957.
[54] O. Saito, On the effect of high energy radiation to polymers I. Cross-linking and degradation, J. Phys. Soc. Jpn. 13 (2) (1958) 198–206.
[55] P. Bracco, V. Brunella, M.P. Luda, M. Zanetti, L. Costailm, Radiation-induced crosslinking of UHMWPE in the presence of co-agents: chemical and mechanical characterisation, Polymer 46 (2005) 10648–10657.
[56] L. Costa, I. Carpentieri, P. Bracco, Post electron-beam irradiation oxidation of orthopaedic UHMWPE, Polym. Degrad. Stab. 93 (9) (2008) 1695–1703.
[57] S.F. Edwards, T. Vilgis, The effect of entanglements in rubber elasticity, Polymer 27 (4) (1986) 483–492.
[58] A. Pawlak, A. Galeski, A. Rozanski, Cavitation during deformation of semi-crystalline polymers, Prog. Polym. Sci. 39 (5) (2014) 921–958.